Programmable cesium Rydberg wave packets

D. W. Schumacher,[1] J. H. Hoogenraad,[2] Dan Pinkos,[3] and P. H. Bucksbaum[1]
[1]*Physics Department, University of Michigan, Ann Arbor, Michigan 48109*
[2]*FOM-Institute for Atomic and Molecular Physics, Amsterdam, The Netherlands*
[3]*Center for Ultrafast Optical Science, University of Michigan, Ann Arbor, Michigan 48109*
(Received 10 July 1995)

We have used amplified, programmable, shaped optical pulses to engineer Rydberg wave packets in cesium. Our apparatus employs a computer-controlled liquid-crystal pulse shaper which could control either the phase or the magnitude of the pulse's spectrum. The shaped optical field was analyzed via cross correlation and frequency-resolved optical gating. The wave-packet evolution was analyzed by monitoring temporal interference via the optical Ramsey method to obtain both auto- and cross-interferograms of the engineered wave packet.

PACS number(s): 32.80.Rm

I. INTRODUCTION

We have tailored an atomic Rydberg wave function by controlling the spectrum and phase of the excitation radiation. Our apparatus employs a 10-nm bandwidth coherent optical pulse generated by a Kerr lens mode locked laser (KLM), which is shaped using a computer-controlled segmented liquid-crystal modulator (LCM). Following amplification, the shaped light excites a coherent superposition of np states (a wave packet) in atomic cesium. Both the magnitude *and phase* of the complex scalar field $\Psi(r,t)$ can be controlled in this way. We examine the shaped wave function in two ways: the optical Ramsey method [1,2] produces an autocorrelation of $\Psi(r,t)$, which can be used to derive its spectrum. A related technique is the "cross interferogram," which is a phase-sensitive monitor of the wave packet.

This research was motivated by our interest in the problem of coherent control of quantum processes [3]. A wave packet affords control by localizing the electron probability amplitude where it is wanted. As a simple example, ionization from an intense, short pulsed laser can be suppressed by keeping the wave function away from the core of the atom. In this paper we show how light may be shaped to control wave-packet formation. Wave-packet shaping using shaped optical pulses made with a fixed mask [4] has been demonstrated as has shaping using unshaped pulses, but utilizing various aspects of the light-atom interaction [5].

This paper is organized as follows. Section II describes the experimental apparatus for shaping and characterizing the optical pulses used in the experiment. The wave-packet evolution is monitored by measuring auto- and cross-interferograms using the optical Ramsey method, which is discussed in Sec. III. The apparatus implementing the method is described in Sec. IV. The results of this work are presented and discussed in Sec. V. Finally, Sec. VI summarizes the experiment and outlines future experiments.

II. OPTICAL PULSE SHAPING AND MEASUREMENT

Our pulse shaper is a frequency domain device that resembles two back-to-back spectrometers [6]. Briefly, the first spectrometer consists of a diffraction grating followed by a spherical mirror (Fig. 1). For collimated input light, the image plane of the spectrometer is the focal plane of the mirror (the Fourier plane). This forms the input plane of the second spectrometer, which is a mirror image of the first, i.e., a spherical mirror followed by a grating. The second spectrometer recombines the dispersed colors, so that ideally the system has zero spatial and temporal dispersion. The pulse is shaped by a programmable phase or amplitude mask placed in the Fourier plane.

The first optical pulse shaper of this type used fixed (nonprogrammable) masks, which could modify amplitude or phase [6]. The use of a programmable LCM phase mask was first reported in 1990 [7]. The first demonstration of LCM-based phase and amplitude shaping was reported in 1993 [8]. Recently, shaping using an acousto-optic modulator in the Fourier plane was demonstrated [9].

The LCM pulse shaper used in this experiment was constructed at the National Science Foundation Center for advanced liquid crystalline optical materials (ALCOM) at Kent State University. It used a positive nematic liquid crystal sandwiched between two glass plates patterned with indium

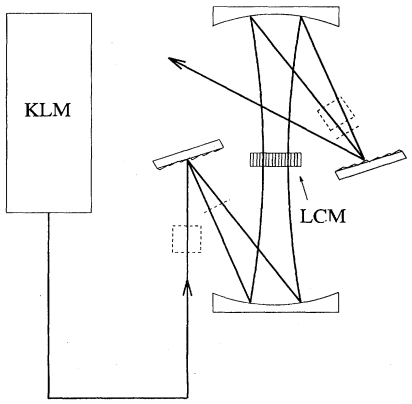

FIG. 1. Pulse shaping apparatus. The hardware used for phase shaping is shown in solid lines. Addition of the dashed elements (box denotes polarizer, line denotes half-wave plate) allows for amplitude shaping.

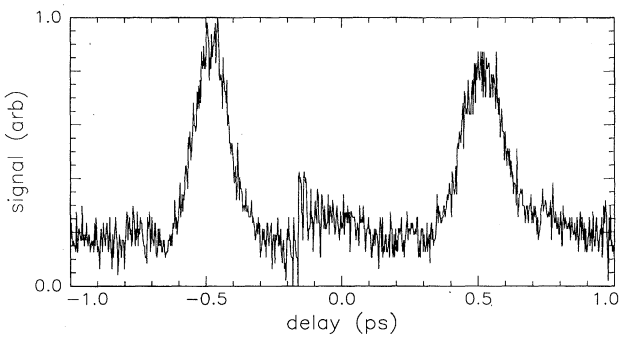

FIG. 2. Cross correlation of a phase shaped pulse with the unshaped pulse from which it was generated. The phase shaping involved sudden π phase jumps with a periodicity 16 LCM pixels. The abscissa is the delay between the shaped and unshaped pulses in the cross-correlator.

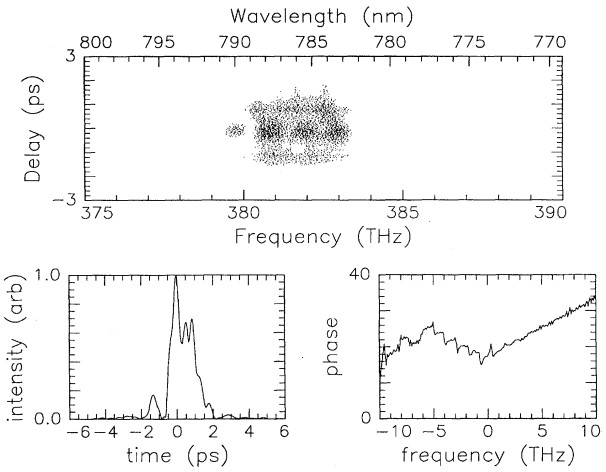

FIG. 3. FROG results for a shaped pulse: π phase jumps, 16 pixel period. Shown are the FROG image (top), extracted intensity (left), and electric field phase (right). Note the phase is shown as a function of *frequency* so the operation of the LCM may be seen.

tin oxide (ITO) to make electrical contact. The director, which defines the optic axis of the anisotropic liquid, was oriented parallel to the device's width and, in the absence of a field, had a constant orientation throughout the crystal. There were 256 individual pixels, each 300 μm wide by $\sim$1 cm high. The pixels were arranged side-by-side giving the unit's active area a total width just over 7.5 cm. Each pixel width includes a 10% ($\sim 30\mu$m) dead space, that is, an area in between the patterned ITO electrodes. In the absence of fringing fields, this area will simply transmit the light passing through it unaltered. The LCM was controlled by two Cambridge Research Instruments (CRI) drivers, each capable of addressing 128 pixels. The drivers were themselves controlled by a personal computer.

The LCM was configured as a phase shaper by placing it between pairs of gratings and mirrors as described above and as depicted in Fig. 1. The system used gold-coated, holographic gratings with 2000 lines/mm and spherical aluminum mirrors with a focal length of 500 mm. The diffraction limited spot size for this system is 5 μm, 6 times smaller than the LCM pixel size. We used 100-fs pulses with approximately 10 nm of bandwidth centered about 790 nm from a KLM titanium sapphire laser. This was collimated in a telescope, and then injected at an incident angle of 76° to the first grating, with p polarization. The gratings pass p polarization preferentially over s polarization with a contrast of roughly 30:1. Light propagating through the system suffered roughly 50% losses from light reflected into the zero-order grating mode, absorption in the aluminum mirror coating, and surface reflections from the LCM. The temporal shape of the light was unaltered when the LCM was not powered. When powered, each pixel could shift the phase of the radiation "addressed" over a range exceeding 2π, providing phase control of the radiation within the resolution of our system. The resolution is determined by the grating, lens, and pixel width, and was 0.12 THz/pixel.

Figure 1 also shows the same LCM configured as an amplitude shaper. A Glan-Thompson polarizer was placed before the first grating to improve the polarization purity of the light injected into the system. A half-wave plate then rotated the polarization to 45° with respect to the director. A polarizer followed, aligned to extinguish the light when the LCM was not powered. A wave plate following the second polarizer rotated the polarization back to the p axis. Each pixel, then, acted as a programmable half-wave plate between two crossed polarizers, allowing amplitude control of the short pulses generated by our KLM. This method of amplitude modulation also introduces an additional phase shift equal to half the difference in phase between the fast and slow axes of the liquid crystal. If necessary, this can be eliminated using a second LCM phase modulator [8], however our experiment did not require this. After shaping, the pulses were amplified up to 10 mJ using chirped-pulse amplification [10] at a repetition rate of 10 Hz. Care was taken to operate the amplifier in an unsaturated, linear gain regime, in order to not distort the pulse.

Prior to amplification, the shaped pulses were characterized with a monochromator and cross-correlator. These devices are useful diagnostics, but they do not allow complete determination of the pulse shape. After amplification, the greater energies available allowed us to exploit a new technique, frequency-resolved optical gating (FROG) [11], that provides total determination of a short pulse to within a few trivial phase ambiguities. The phase shaped pulses were measured using FROG and a deconvolution algorithm employing intensity constraints [12] and generalized projections [13]. It would have been difficult to characterize these pulses any other way, given their complex phase variation.

A typical cross correlation is shown in Fig. 2 for an LCM phase "mask" consisting of a periodic sequence of pixels with alternating 0 and π phase shifts. The principal effect is to split the injected pulse into two pulses with a time separation given by the reciprocal of half the periodicity in frequency $(\Delta f \times n/2)^{-1}$. The mask had a periodicity of 16 pixels, or equivalently, 1.92 THz. This resulted in a splitting of 1.10 ps, which compares well with the predicted value of 1.04 ps. This double pulse *could not* have been created using a simple beam splitter and delay line in an interferometer

configuration. The phase relationships between the two pulses are different. An interferometer uses a linear phase sweep to translate one pulse with respect to the other. Here, the pulse shaper is using sudden phase jumps.

Figure 3 shows the results of FROG analysis on the phase shaped pulse after amplification. Although Fig. 2 clearly shows a double pulse with separation of 1.1 ps, double pulses are not evident in the FROG results. Nonetheless, the extracted phase data have phase jumps of nearly π. The change in shape is due to a spectral shift in the amplifier. The spectrum must be centered over a phase jump to obtain clearly resolved pulses, or the various frequency components will not balance to create the null between the two pulses. The phase jumps were centered before amplification; however, the amplifier system pulled the frequency spectrum slightly so that the symmetry was broken. This was not corrected because we only required the π jumps to be present for this experiment, the centering not being important. There is also a spectral cubic phase error due to uncompensated higher-order dispersion in the amplifier. Note the bandwidth of these pulses is less than the system is capable of providing because the wings are clipped somewhat to excite fewer states in the wave-packet experiment to be described later.

III. TIME DOMAIN RAMSEY METHOD: AUTO- AND CROSS-INTERFEROGRAMS

We required a means of detecting the changes in the wave packet formed in the cesium as the light exciting it was shaped. Currently, no method for measuring the spatial variation of an atomic wave packet has been demonstrated. Although a wave packet has been measured completely recently in Na_2 using tomography [14], the method took advantage of the harmoniclike potential wells present in that molecule and is not readily generalized to atoms. The amount of wave function near the core can be measured via short pulse photoionization, and this was the principal means used to measure wave packets when the experiments forming them first took place [15]. In general, these experiments present formidable signal-to-noise problems because short pulse lasers cannot saturate the ionization of Rydberg states with Kepler times longer than the pulse duration.

A somewhat different technique monitors wave-packet *evolution* by comparing it to a reference wave packet [1,2]. We use this approach to examine wave packets produced with amplitude-shaped light. The method has been variously described as a Ramsey technique and as atomic interferometry. The former refers to the use of two fields that are phase coherent and separated in time, much as Ramsey's method uses two phase-coherent fields separated in space. A pulse is injected into a Michelson interferometer, which splits it into two identical pulses with a variable delay between them. The pulse pair is then used to excite an atom. The wave packet excited by the first pulse evolves and, subsequently, has changed shape and location by the time the second wave packet is launched. As the delay between the two pulses changes, the population excited by each of the two pulses will interfere constructively and destructively, causing variations in the yield.

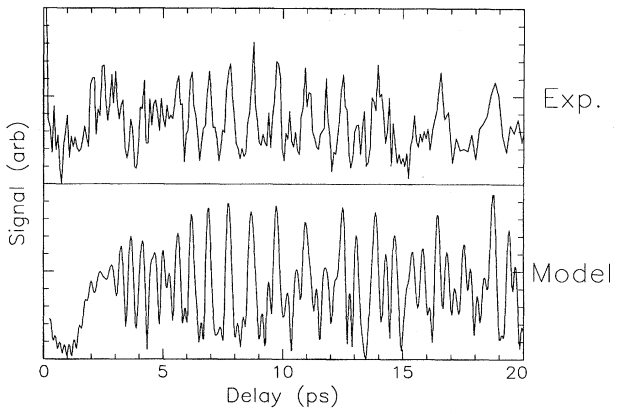

FIG. 4. Interferogram using an unshaped pulse: experimental results (top) and model calculation (bottom).

The total Rydberg wave function can be written as (in atomic units)

$$|\Psi(t,\vec{r})\rangle=\sum_n c_n(t)e^{-i\omega_n t}|n\rangle, \tag{1}$$

where the c_n are the complex amplitudes and the ω_n the energies of the eigenstates $|n\rangle$. Let $E(t)$ represent the (complex) optical field of a single pulse. According to first-order perturbation theory, and using the rotating-wave approximation, the total amplitude of state n after both pulses is

$$c_n(\tau)=\frac{i\mu_n}{2}\int_{-\text{infinity}}^{\text{infinity}}[E(t)+E(t+\tau)]e^{-i\Delta_n t}dt, \tag{2}$$

where μ_n is the dipole moment connecting the initial state to $|n\rangle$, and Δ_n is the energy difference $\omega_{\text{initial}}-\omega_n$. Denoting the Fourier transform of $E(t)$ with respect to Δ_n as $\bar{E}(\Delta_n)$, and the delay as τ, we have

$$\begin{aligned}|c_n|^2&=\frac{\mu_n^2}{4}|\bar{E}(\Delta_n)+\bar{E}(\Delta_n)e^{i\Delta_n\tau}|^2\\&=\frac{\mu_n^2}{2}|\bar{E}(\Delta_n)|^2(1+\cos\Delta_n\tau).\end{aligned} \tag{3}$$

The total population P is

$$P(\tau)=|\Psi|^2=\sum_n |c_n|^2. \tag{4}$$

As τ is varied, P will undergo complex oscillations as the n frequencies present beat against each other. If we introduce a nonlinearity, we can measure the envelope within which the oscillations occur. One way to do this is to evaluate the root-mean-square (RMS) variation of (4) [1]. Figure 4 (bottom) shows the RMS variation for the case of excitation by a model, short, Gaussian pulse.

There are some important time scales characterizing the evolution of a wave packet [16]. The time for a particle in an equivalent classical system to execute one orbit is

$$T_k = 2\pi\left(\frac{\partial E_n}{\partial n}\right)^{-1} = 2\pi n^{*3}, \tag{5}$$

where E_n is the energy of the state with principal quantum number n, and n^* is the effective quantum number given by $-1/\sqrt{2E_n}$. The quadratic dependence of E on n introduces dispersion in the wave-packet evolution, causing the wave packet to explore regions of phase space that a similar wave packet in a harmonic oscillator would never see. The revival time, T_r, is the time for this wave packet to return to the phase space of the harmonic oscillator [16]. The revival time is given by

$$T_r \approx 2\pi\left(\frac{\partial^2 E_n}{\partial n^2}\right)^{-1} = T_k^2\left(\frac{\partial T_k}{\partial n}\right)^{-1} = \frac{2}{3}\pi n^{*4}. \tag{6}$$

If pulses used are short compared to the Kepler time, the signal in Fig. 4 has an interesting interpretation [1] because each pulse alone produces a well-localized wave packet. Near $\tau = \frac{1}{2}T_k$ the first wave packet is localized at the outer turning point of the classical orbit, so that the two wave packets occupy different locations. Thus there is no quantum interference, so the total population is relatively independent of delay, resulting in the small RMS value near 1 ps. Near $\tau = T_K$, on the other hand, the two wave packets are both at the core, the first having just completed its first circuit. The two wave packets interfere, so that a large RMS value seen around 2.5 ps. Somewhat after the first return of the wave packet, at $\frac{1}{2}T_r$, we see a series of peaks spaced by $\frac{1}{2}T_K$. The wave packet has dispersed into two equally spaced sub-wave packets. This is called a "fractional revival."

The above interpretation is appealing, and correct if it is known that short pulses are indeed being used. However, from (3), we see that only the spectral magnitude appears, not the spectral phase. A short pulse would yield the same signal as a severely chirped pulse, for example [17]. Independent of the pulse shape, we can still say that the RMS signal reports how similar two wave packets are, so that an atomic interferogram monitors the *evolution* of the wave packet [1]. The peak occurring at a delay equal to the Kepler orbit time represents the first return of the wave packet to its initial conditions, and similarly for the various fractional revivals. The interferogram, then, is a time domain view of the atomic spectrum.

Since the autointerferogram is equivalent to a Fourier transform of the spectrum, it can be used to record changes in amplitude-shaped light. Clearly, however, it is not useful for detecting phase shaping. Two ways around this difficulty are suggested by analogy with optical interferometry. The optical interferogram (field autocorrelation) from a Michelson interferometer is also phase independent. It measures only a coherence length (spectral magnitude dependent only), as opposed to a pulse width (magnitude and phase dependent). One way to improve things is to introduce a nonlinearity, for example, add a doubling crystal to make a second order, intensity autocorrelator. Another way is to break the symmetry in the system and interfere one pulse with a different reference pulse. We can make the atom nonlinear by using more intense light. We have done this recently in potassium [2]. In cesium, however, the coupling between the initial state and the Rydberg states is weak (a typical dipole matrix element is about 0.02 atomic unit), and increasing the intensity produces considerable ionization. A cross-interferogram is simpler, and this was the method used. Specifically, we measured cross-interferograms formed by interfering a reference, unshaped, wave packet with a shaped one. As is the previous argument, if the reference wave packet is short compared to the Kepler time, the cross-interferogram can be interpreted as a measure of the amount of shaped wave packet near the core.

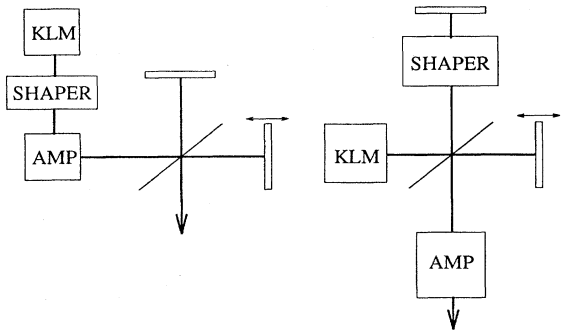

FIG. 5. Apparatus for measuring autointerferograms (left) and cross-interferograms (right).

IV. APPARATUS FOR MEASURING THE INTERFEROGRAMS AND THE ATOMIC SYSTEM

The system used to measure the evolution of amplitude shaped pulses is shown in Fig. 5 (left). The light from the KLM is amplitude shaped and amplified, then injected into a Michelson interferometer forming the pulse sequence necessary to measure an autointerferogram. One leg of the Michelson had a computer controlled length which could change in 1-μm increments corresponding to a delay change of 6.7 fs. The optical period for this experiment was about 2.6 fs. Since we were only interested in the RMS envelope, there was no need to follow the evolution with sub-optical-cycle resolution. It was sufficient to change the delay on a scale that was small compared to the slow variations of the envelope. Although this technique does not require the Michelson to be stable, the one used to generate the autointerferogram was, in fact, stable to better than one-quarter of a wave.

The light illuminated an effusive cesium beam inside a vacuum chamber. Typically, each pulse had an energy of about 200 μJ and a spot size of about 3 mm at the interaction region. The chamber had a base pressure of 5×10^{-7} torr. The beam was formed by heating a stainless steel oven containing 3–10 g of cesium to 100–150 °C. The vapor from the molten cesium (melting point 28.7°) passed through two apertures, one on the oven itself, the other about 2 cm away, forming a beam. The aperture sizes were approximately 0.4 and 3 mm, respectively. The atomic beam passed between and parallel to two capacitor plates, orthogonal to the laser beam.

Just prior ($\sim$4 ns) to excitation with the shaped light, the cesium was excited from the $6s$ ground state to the $7s$ state using 1.079-μm light to drive a two-photon transition. The

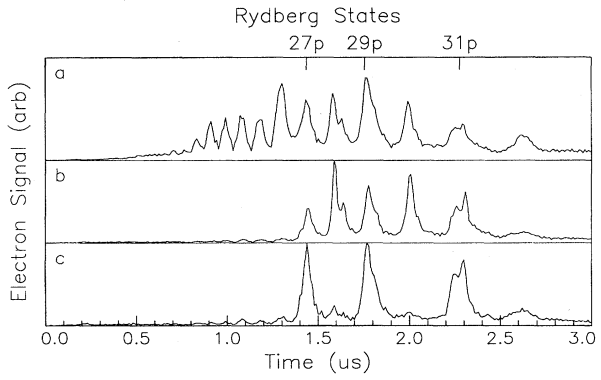

FIG. 6. Rydberg spectrum excited by (a) unshaped, (b) windowed, and (c) sliced pulses. The spectrum was measured using ramped field ionization. Higher np states, being less bound, appear first.

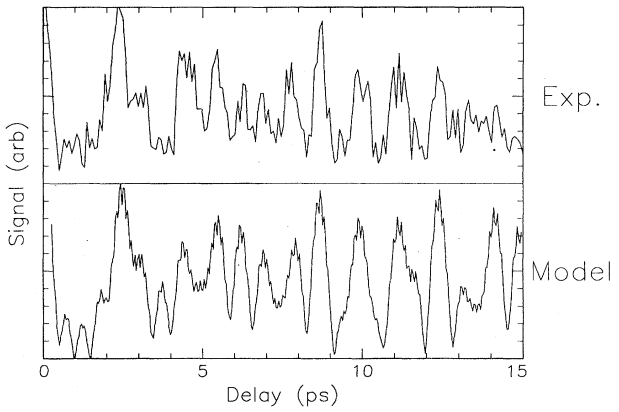

FIG. 7. Autointerferogram exciting with a windowed pulse.

lifetime of the $7s$ state is about 7 ns. The infrared light was generated by difference frequency mixing the 1.06-μm fundamental of an Nd:YAG laser with 535.7-nm light from an amplified, Hansch dye laser in a Type I KD*P crystal. The output of the Hansch laser was about 4 mJ, which yielded about 200 μJ of 1.079-μm light when mixed with 20 mJ of the Nd:YAG fundamental. The infrared and short pulsed light were both polarized normal to the capacitor plates.

After excitation by both lasers, the total population was measured at a given delay using ramped field ionization [18]. A high-voltage pulser delivered a $\sim$3-kV negative going pulse with a 3-μs rise time to one of the capacitor plates. The other plate had 0.4-mm hole in it leading to a double microchannel plate detector after a 4-cm drift region. The capacitor plate spacing was 1 cm. The pulsed voltage field ionized the Rydberg states with nearly 100% efficiency and drove the resulting electrons to the detector. The high efficiency is one of the important advantages of this method over using ionization to study wave-packet behavior. Both the infrared and short pulsed light used to excite the cesium were polarized parallel to the ramped field.

Each Rydberg state, bound by a different energy, was ionized at a different voltage and hence, a different time. This allowed us to distinguish different Rydberg states and was a useful diagnostic. A typical field ionization profile from an unshaped, short pulse is shown in Fig. 6(a). We measured the RMS of the signal integrated over all the Rydberg states as a function of delay to construct an interferogram. Typically, each data point consisted of the RMS of the signal from six different delays 6.7 fs apart. That is, if the signal for the ith delay is denoted x_i, then the RMS signal was

$$\mathscr{S}_{\rm rms}=\left[\frac{\Sigma_{i=1}^{6}x_i^2}{6}-\left(\frac{\Sigma_{i=1}^{6}x_i}{6}\right)^2\right]^{-1/2}. \tag{7}$$

A laser shot was used only if each excitation laser was within $\sim\pm 7\%$ of some given value. The delay range measured ranged from about -15 to $+15$ ps. The autointerferograms were symmetric about zero delay, as they should be, so the results for positive and negative delays were averaged to improve the signal-to-noise ratio.

The apparatus for using phase shaped light is shown in Fig. 5 (right). The cross-interferogram compares a shaped pulse to a near-transform-limited reference pulse. Since the latter generates a wave packet localized near the core, the cross-interferogram is the time-dependent current of the phase shaped wave packet near the core. To construct a cross-interferogram, the phase shaper shown in Fig. 1 was inserted into one leg of the Michelson interferometer. The size of the shaper required that each leg of the interferometer be 2 m long, so the long-term stability was greatly reduced. However, as we have already noted, long-term interferometric stability is not crucial for the measurement. The two-pulse output was amplified as before.

V. RESULTS AND DISCUSSION

The autointerferogram of a short, unshaped pulse is shown in Fig. 4 (top), to be compared with the model interferogram shown below. The first return and some of the fractional revivals stand out clearly. The first use of the amplitude shaper was simply to limit the number of states contributing by "windowing" the optical spectrum. The resultant Rydberg spectrum is shown in Fig. 6(b). The measured autointerferogram and model calculation are presented in Fig. 7. The first return is cleaner after the pulse is spectrally windowed. Fewer states are excited so the wave packet suffers less dispersion, and much of the fast structure present in the autointerferogram of the unshaped pulse is removed. The match between experiment and model is much improved.

The high intensities used in this experiment meant that there could be effects beyond the first-order perturbation theory predictions (3) and (4). As a check, Schrödinger's coupled equations of motion were integrated using an essential state basis consisting of the $7s$ initial state and 20-Ry np states. No continuum states were used, so ionization was not included. The equations were

$$\dot{c}_i(t)=\frac{-i}{2}\sum_n c_n(t)\langle n|z|i\rangle A(t)e^{i(\omega_0-\Delta_n)},$$

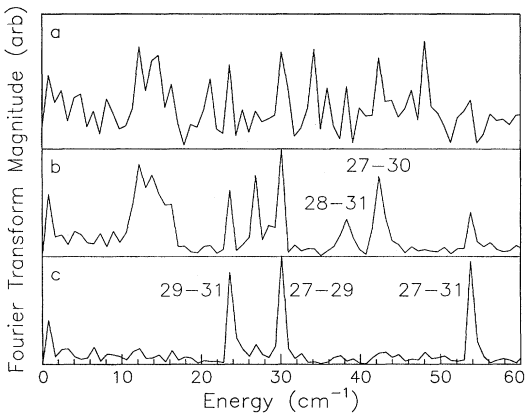

FIG. 8. Fourier transforms of the interferograms made using (a) unshaped, (b) windowed, and (c) sliced pulses. Each peak corresponds to the energy spacing between two Rydberg states. A few peaks have been labeled.

$$\dot{c}_n(t) = \frac{-i}{2} c_i(t) \langle i|z|n\rangle A^*(t) e^{-i(\omega_0 - \Delta_n)}, \tag{8}$$

where c_i is the amplitude for the initial $7s$ state, and the electric field is represented as a complex envelope $A(t)$ over a carrier wave with frequency ω_0. The matrix elements were evaluated using Numerov numerical integration to find the cesium wave functions given the known quantum defects (about 4.08 for $7s$ and 3.56 for np). The results of (4) and (8) were in close agreement, indicating that even for the largest fluence used in this experiment, the system was still essentially perturbative. In any case, all model interferograms shown were calculated using (8).

An experimental check was also made. If the system is described well by lowest-order perturbation theory, then the $7s$ state is not significantly depleted, and each *individual Rydberg state* should have a population that oscillates like a simple sine wave at frequency $\omega_n - \omega_{7s}$. The analysis indicated small nonperturbative effects (other difference frequencies), but the system was mostly in the weak response limit.

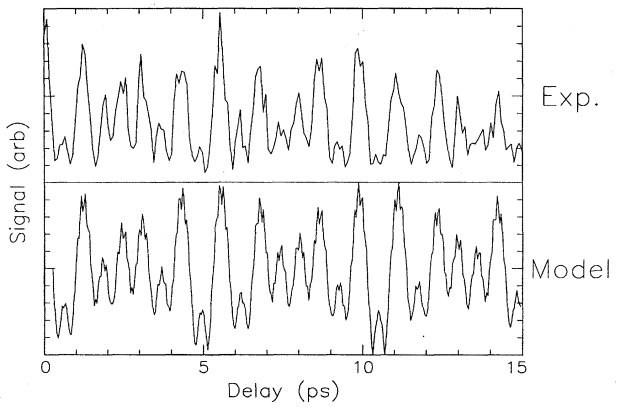

FIG. 9. Autointerferogram exciting with a sliced pulse.

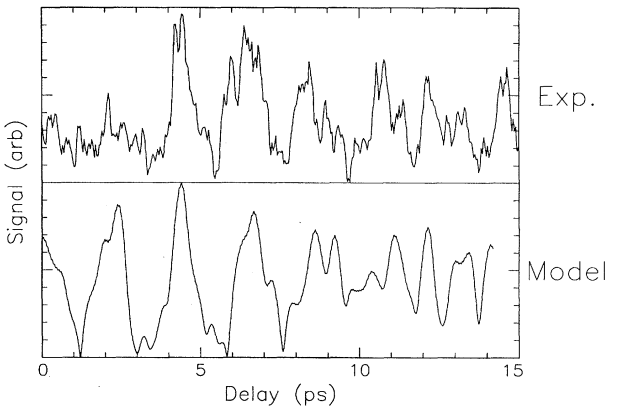

FIG. 10. Cross-interferogram exciting with a phase shaped pulse.

The Fourier transform of an interferogram, on the other hand, will have peaks at many of the difference frequencies possible in the system. Only the differences between Rydberg states appear, as opposed to their separation from the initial state, because of the RMS process. Fourier transforms of the interferograms made using the unshaped and windowed pulses are shown in Figs. 8(a) and 8(b). Since the autointerferograms were measured over 30 ps of delay, the spectral resolution was about 1 cm^{-1}. The spacings between Rydberg states are clearly well resolved and could be unambiguously identified. Several are labeled in the figure. Note the simpler spectrum of the windowed data.

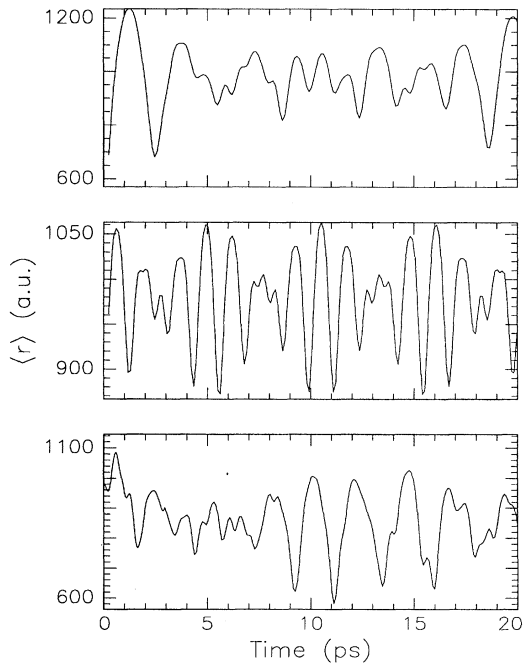

FIG. 11. Calculated wave-packet evolution of an (a) unshaped wave packet, (b) sliced wave packet, and (c) phase shaped wave packet. The radial expectation value $\langle r \rangle$ is plotted in atomic units as a function of time in ps.

We next used the amplitude shaper to window and "slice" the optical spectrum to produce the Rydberg spectrum shown in Fig. 6(c). The only states excited were $27p$, $29p$, and $31p$. The spectrum was also shaped to equalize the populations (given by the integral under the peaks, not the height). The measured interferogram and model calculation are shown in Fig. 9. Note that the first return now occurs at about one-half the Kepler orbit time. Effectively, the spacing between states has doubled, so the relevant times, including the recurrence time, have halved approximately. There is also less dispersion present, of course. The Fourier transform is shown in Fig. 8(c). The only three possible state separations are all present.

We used phase shaping to change the initial conditions with which the wave packet was launched. The shaped pulse had a series of sharp π phase jumps occurring periodically in its frequency spectrum, as described previously, and caused equivalent phase jumps in the Rydberg states excited. We measured the effect of these jumps by measuring the cross-interferogram using an amplified unshaped pulse to create a reference wave packet. Figure 10 shows the result when exciting with the shaped pulse. The shaped wave packet begins dispersed and immediately launches into a series of recurrences. A model calculation is shown as well. The calculation does not agree as well for the phase shaped results as for the amplitude shaped ones because small misalignments in the various grating systems used in the laser system cause frequency sweeps across the spatial mode that can result in the FROG measuring a somewhat different pulse than that used in the experimental vacuum chamber.

Finally, to help summarize the results from using the different shaped pulses, Fig. 11 shows the calculated expectation value of the radial coordinate, $\langle r \rangle$, as a function of time for excitation by an unshaped pulse, the sliced pulse, and the phase shaped pulse. When the wave packet is localized the behavior is nearly classical and $\langle r \rangle$ describes a classical trajectory with strong modulations. When the wave packet delocalizes, the modulations are vastly reduced. As expected, the time variation of the wave packet excited by the sliced pulse is roughly twice as fast (note the first return) than that for the unshaped pulse. The behavior of the wave packet excited by the phase shaped pulse, on the other hand, is different in a completely different way. It reaches its full revival in approximately half the time compared to the unshaped wave packet, although the Kepler time is unchanged. This is because the entire interferogram has been shifted in phase.

VI. CONCLUSION

This paper has presented results of the use of amplitude and phase shaped light to excite shaped wave packets. The wave-packet evolution was monitored using autointerferograms and, for the first time, cross-interferograms. By using phase and amplitude shaping it was possible to engineer new structures in the wave-function probability distribution, and measure them. The amplitude shaped pulses were used to control the time scales characterizing the wave-packet evolution, the phase shaped pulse was used to shift specific features in the wave packet's evolution to a different time. Interesting issues to explore now include the effect of depletion and other strong response effects on wave-packet evolution and control. Also, by using simultaneous phase and amplitude shaping, it should be possible to craft more complicated structures in the target wave function [19]. Finally, we would also like to exploit the computer control of these LCM optical pulse shapers to implement learning algorithms that use feedback from the experiment to control the shape of the wave packet [20].

ACKNOWLEDGMENTS

We wish to acknowledge the assistance of the National Science Foundation Center for Advanced Liquid Crystalline Optical Materials (ALCOM) at Kent State University. We also thank R. R. Jones, M. L. Naudeau, and C. I. Sukenik for their advice during this work. Rick Trebino and K. W. DeLong gave us considerable help in implementing their FROG technique. This work was supported by the National Science Foundation. J.H.H. participated through the Fellows Program of the Center for Ultrafast Optical Science, and FOM Institute, supported by the Netherlands Organization for the Advancement of Research.

[1] N. F. Scherer, A. J. Ruggiero, M. Du, and G. R. Fleming, J. Chem. Phys. **93**, 856 (1990); L. D. Noordam, D. I. Duncan, and T. F. Gallagher, Phys. Rev. A **45**, 4734 (1992); B. Broers *et al.* , Phys. Rev. Lett. **71**, 344 (1993); B. Broers, J. F. Christian, and H. B. van Linden van den Heuvell, Phys. Rev. A **49**, 2498 (1994).

[2] R. R. Jones, C. S. Raman, D. W. Schumacher, and P. H. Bucksbaum, Phys. Rev. Lett. **71**, 2575 (1993).

[3] For a brief review see Warren S. Warren, Herschel Rabitz, and Mohammmed Dahleh, Science **259**, 1581 (1993).

[4] B. Broers, L. D. Noordam, and H. B. van Linden van den Heuvell, Phys. Rev. A **46**, 2749 (1992).

[5] L. D. Noordam, H. G. Muller, A. ten Wolde, and H. B. van Linden van den Heuvell, J. Phys. B **23**, L115 (1990); R. R. Jones and P. H. Bucksbaum, Phys. Rev. Lett. **67**, 3215 (1991); J. H. Hoogenraad, R. B. Vrijen, and L. D. Noordam, Phys. Rev. A **50**, 4133 (1994).

[6] J. P. Heritage, A. M. Weiner, and R. N. Thurston, Opt. Lett. **10**, 609 (1985).

[7] A. M. Weiner, D. E. Leaird, J. S. Patel, and J. R. Wullert, Opt. Lett. **15**, 326 (1990).

[8] Marc M. Wefers and Keith A. Nelson, Opt. Lett. **18**, 2032 (1993).

[9] C. W. Hillegas *et al.*, Opt. Lett. **19**, 737 (1994).

[10] D. Strickland and G. Mourou, Opt. Commun. **56**, 219 (1985).

[11] Rick Trebino and Daniel J. Kane, Opt. Soc. Am. A **10**, 1103 (1993); K. W. DeLong, Rick Trebino, and Daniel J. Kane, J. Opt. Soc. Am. B **11**, 1595 (1994).

[12] K. W. DeLong and Rick Trebino, J. Opt. Soc. Am. A **11**, 2429 (1994).
[13] Kenneth W. DeLong *et al.*, Opt. Lett. **19**, 2152 (1994).
[14] T. J. Dunn, I. A. Walmsley, and S. Mukamel, Phys. Rev. Lett. **74**, 884 (1995).
[15] A. ten Wolde *et al.*, Phys. Rev. Lett. **61**, 2099 (1988); John A. Yeazell, Mark Mallalieu, Jonathan Parker, and C. R. Stroud, Jr., Phys. Rev. A **40**, 5040 (1989).
[16] Jonathan Parker and C. R. Stroud, Jr., Phys. Rev. Lett. **56**, 716 (1986); I. Sh. Averbukh and N. F. Perelman, Phys. Lett. A **139**, 449 (1989).
[17] R. R. Jones, D. W. Schumacher, T. F. Gallagher, and P. H. Bucksbaum, J. Phys. B **28**, L405 (1995).
[18] See, for example, Thomas F. Gallagher, *Rydberg Atoms* (Cambridge University, New York, 1994).
[19] D. J. Tannor and S. A. Rice, J. Chem. Phys. **83**, 5013 (1985); Jeffrey L. Krause *et al.*, J. Chem. Phys. **99**, 6562 (1993); J. L. Krause, K. R. Wilson, and Y. J. Yan, *Laser Techniques for State-Selected Chemistry II*, edited by J. W. Hepburn (SPIE—International Society for Optical Engineering, Bellingham, WA, 1994), p. 258; B. Kohler *et al.*, Accts. Chem. Res. **28**, 133 (1995).
[20] Richard S. Judson and Herschel Rabitz, Phys. Rev. Lett. **68**, 1500 (1992).